Biogeosciences Discuss., 12, 8429–8465, 2015
www.biogeosciences-discuss.net/12/8429/2015/
doi:10.5194/bgd-12-8429-2015

Biogeosciences Discussions
Open Access

Carbonate saturation state of surface waters in the Ross Sea and Southern Ocean: controls and implications for the onset of aragonite undersaturation

H. B. DeJong, R. B. Dunbar, D. A. Mucciarone, and D. A. Koweek

Department of Earth System Science, Stanford University, Stanford, CA, USA

Received: 6 May 2015 – Accepted: 12 May 2015 – Published: 8 June 2015

Correspondence to: H. B. DeJong (hdejong@stanford.edu)

Published by Copernicus Publications on behalf of the European Geosciences Union.

Abstract

Predicting when surface waters of the Ross Sea and Southern Ocean will become undersaturated with respect to biogenic carbonate minerals is challenging in part due to the lack of baseline high resolution carbon system data. Here we present ~1700 surface total alkalinity measurements from the Ross Sea and along a transect between the Ross Sea and southern Chile from the austral autumn (February–March 2013). We calculate the saturation state of aragonite (Ω_{Ar}) and calcite (Ω_{Ca}) using measured total alkalinity and pCO_2. In the Ross Sea and south of the Polar Front, variability in carbonate saturation state (Ω) is mainly driven by algal photosynthesis. Freshwater dilution and calcification have minimal influence on Ω variability. We estimate an early spring surface water Ω_{Ar} value of ~1.2 for the Ross Sea using a total alkalinity–salinity relationship and historical pCO_2 measurements. Our results suggest that the Ross Sea is not likely to become undersaturated with respect to aragonite until the year 2070.

1 Introduction

Atmospheric CO_2 concentrations have increased by 40 % since preindustrial times to ~400 ppm today and could double by the year 2100 (IPCC AR5 WG1, 2013). Due to oceanic uptake of CO_2, the pH of surface waters of the world's oceans are projected to decrease by 0.3–0.4 units by the end of the century, equivalent to a 50 % decrease in carbonate ion (CO_3^{2-}) concentrations (Orr et al., 2005). Even after CO_2 emissions are halted, it will take thousands of years before the surface ocean pH returns to the preindustrial state (Caldeira and Wickett, 2003; Archer et al., 2009).

The saturation state (Ω) of seawater with respect to a specific calcium carbonate ($CaCO_3$) mineral (aragonite, calcite, or magnesium calcite) is defined as:

$$\Omega = \frac{[Ca^{2+}]\left[CO_3^{2-}\right]}{K_{sp}} \quad (1)$$

BGD
12, 8429–8465, 2015

where K_{sp} is the solubility product constant for the specific $CaCO_3$ mineral and depends on salinity, temperature, and pressure (Mucci, 1983). Aragonite is ~ 1.6 times more soluble than calcite at 0 °C whereas the solubility of magnesium calcite varies depending on the mole fraction of magnesium ions (Dickson, 2010). Ω_{Ar} represents the saturation state of aragonite and Ω_{Ca} represents the saturation state of calcite. $\Omega < 1$ represents undersaturation where dissolution is thermodynamically favorable and $\Omega > 1$ represents supersaturation where precipitation is favorable. Most surface waters of the global oceans are currently supersaturated with respect to $CaCO_3$ (Feely et al., 2009). However, decreasing CO_3^{2-} concentrations can decrease calcification rates even in supersaturated conditions (e.g. Moy et al., 2009; Andersson et al., 2011).

The Southern Ocean is especially vulnerable to Ocean Acidification (OA) due to its relatively low total alkalinity (TA) and because of increased CO_2 solubility in cold water. In addition, Antarctic continental shelves have insignificant sedimentary $CaCO_3$ to buffer against OA (Hauck et al., 2013). Surface waters in the Southern Ocean may start to become undersaturated with respect to aragonite by 2050 and be fully undersaturated by 2100 (Orr et al., 2005; Feely et al., 2009). McNeil and Matear (2008) have suggested that wintertime aragonite undersaturation in the Southern Ocean may begin as early as 2030.

OA induced decreases in Ω have potentially serious consequences for Antarctic food webs. In the Ross Sea the aragonitic shelled pteropod *Limacina helicina* is a dominant zooplankton that can reach densities of 300 individuals m^{-3} (Hopkins, 1987; Seibel and Dierssen, 2003; Hunt et al., 2008). Pteropods are important prey for nototheniid fish, which in turn are major prey for penguins, seals, and whales (Foster and Montgomery, 1992; La Mesa et al., 2000, 2004). Pteropods may also be important contributors to the biological pump (Collier et al., 2000; Accornero et al., 2003; Manno et al., 2009). A study by Orr et al. (2005) found that the shell of a subarctic pteropod started to dissolve after 48 h when placed in waters with the level of aragonite saturation expected to occur in the Southern Ocean by 2100. Severe dissolution pitting was observed on live pteropods that were collected from the upper 200 m in the Atlantic sector of the

BGD
12, 8429–8465, 2015

Southern Ocean, from waters that were near undersaturatation with respect to aragonite (Bednaršek et al., 2012).

Other organisms in the Southern Ocean may be negatively impacted by OA include krill (Kawaguchi et al., 2013), foraminifera (Moy et al., 2009), sea urchins (Sewell and Hofmann, 2011), deep sea hydrocorals (Shadwick et al., 2014), coralline algae, sea stars, and brittle stars (McClintock et al., 2011). Conversely non-calcareous phytoplankton may benefit in the Ross Sea in a high pCO_2 world, especially the larger diatom *Chaetoceros lineola* (Tortell et al., 2008; Feng et al., 2009).

There are only a few surface carbon system data sets from the Ross Sea (Bates et al., 1998; Sweeney et al., 2000b; Wattsdotter Björk et al., 2014) that can be used to establish baselines in order to understand the relative importance of the physical, chemical, and biological processes that drive the large spatial and seasonal variability of Ω. With no winter Ω measurements, it is challenging to predict when the Ross Sea will become undersaturated with respect to aragonite and calcite. A model by McNeil et al. (2010) suggests that winter surface waters in the Ross Sea will become undersaturated with respect to aragonite by the year 2045 since sea ice, upwelling of deep water, and short residence times prevent these surface waters from reaching equilibrium with the atmosphere. However, McNeil et al. (2010) indirectly estimated surface winter Ω_{Ar} values by using limited carbon system data from the spring (Sweeney et al., 2000b).

We present ~ 1700 underway TA measurements from the surface waters of the Ross Sea and along a transect across the Southern Ocean from the Ross Sea to southern Chile. By combining the underway TA measurements with pCO_2 data we characterize the complete carbon system and describe patterns and controls on Ω variability. Finally, after establishing a relationship between salinity and TA, we use the Lamont Doherty Earth Observatory (LDEO) pCO_2 database (Takahashi et al., 2009) (available at http://www.ldeo.columbia.edu/res/pi/CO2) to provide an independent estimate of Ross Sea surface water Ω_{Ar} in early spring.

BGD
12, 8429–8465, 2015

2 Study site

The Ross Sea is considered a biological hotspot supporting over 400 benthic species (Smith et al., 2012). During the winter the Ross Sea is mostly covered by sea ice, which begins to clear in November to form the largest polynya in Antarctica. As summer approaches, the Ross Sea supports one of the most productive phytoplankton blooms in Antarctica, accounting for up to half of all primary production over the Antarctic continental shelf (Arrigo and McClain, 1994; Smith and Gordon, 1997; Arrigo and van Dijken, 2003). Photosynthesis reduces the concentration of nutrients and dissolved inorganic carbon (DIC) in the mixed layer, causing Ω to increase in surface waters (McNeil et al., 2010). Once the sea ice reforms during autumn and winter, remineralization of organic matter and deep convective mixing produces a relatively homogeneous water column, causing surface DIC concentrations to increase and Ω to decrease (Gordon et al., 2000; Sweeney et al., 2000b; Petty et al., 2013).

The Southern Ocean is composed of multiple fronts that separate distinct water masses (Rintoul et al., 2001). The most prominent are the Antarctic Polar Front (PF) and the Sub-Antarctic Front (SAF). Circumpolar Deep Water (CDW) upwells south of the PF where it becomes modified into Antarctic surface water (AASW). We define the fronts based on the sea surface temperature (SST) gradient after averaging the underway SST data into 0.25° bins. Following Dong et al. (2006), the PF is defined as the southernmost location at which the SST gradient exceeds 1.5×10^{-2} °C km^{-1}. Following Burling (1961), the SAF is defined as the maximum SST gradient in the SST range of 5–9 °C. During our cruise the PF was located at 65.5° S and the SAF was at 57°

BGD
12, 8429–8465, 2015

3 Methods

3.1 Carbon system measurements

As part of the TRacing the fate of Algal Carbon Export (TRACERS) program, we made continuous measurements of surface water TA in the western Ross Sea aboard the *Nathaniel B Palmer* (NBP13-02) from 13 February through 9 March 2013. In addition, from 19 March to 2 April 2013, we made continuous measurements of surface water TA in transit between the Ross Sea and southern Chile along the cruise track shown in Fig. 1.

Underway TA measurements were conducted using the shipboard uncontaminated continuous flow system with an intake located at ~ 5 m depth. Seawater from the ship's underway system was redirected to the bottom of a 250 mL free surface interface cup flowing at 2 L min^{-1} and was drawn from the bottom of the cup for TA analysis without filtration. The entire system was automated and relatively unattended. The sampling cycle was every 24 min on a custom-configured Metrohm 905 Titrando equipped with three Metrohm 800 Dosino syringe pumps (two 50 mL units for sample handling and rinsing and one 5 mL unit for acid titration). Temperature was measured at the cup and in the titration cell. We used certified 0.1 N HCl provided by A. Dickson (Scripps Institution of Oceanography) for the potentiometric titrations and TA calculations follow Dickson et al. (2003). Since we consumed the certified HCl after ~ 1000 measurements in the Ross Sea, we mixed our own 0.1 N HCl solution for the transect to southern Chile (from 12.1 N HCl, laboratory grade NaCl, and deionized water). We calibrated TA measurements using certified reference materials (CRMs) Batch 122 provided by A. Dickson (Scripps Institution of Oceanography). Our estimated precision for the underway TA measurements from 68 CRM analyses is ±3 µmol kg^{-1} (1 SD).

Outlier TA analyses were identified by taking a running mean and standard deviation of 9 consecutive measurements. A measurement was rejected if (1) the difference between the measurement and mean was greater than twice the standard deviation and

BGD
12, 8429–8465, 2015

(2) the difference between the measurement and mean was greater than 6 µmol kg^{-1}. A total of 65 measurements (out of 1716) were rejected.

Surface pCO_2 measurements were made every 3 min using the LDEO air–sea equilibrator permanently installed on the NBP (data available at http://www.ldeo.columbia.edu/res/pi/CO2). The estimated precision is ±1.5 µatm.

In order to evaluate the controls of seasonal surface Ω_{Ar} variability in the Ross Sea, we made discrete water column TA and DIC measurements at 85 stations using Niskin bottles attached to a 24 bottle rosette from 13 February through 18 March 2013 (Fig. 1a). We collected samples for TA and DIC following the protocols of Dickson et al. (2007) and immediately added saturated mercuric chloride (< 0.1 % by volume). For TA, we ran each sample within 12 h of collection using a second potentiometric titrator, a Metrohm 855 Robotic Titrosampler equipped with two 800 Metrohm Dosino syringe pumps (one 50 mL unit for rinsing and sample handling and one 5 mL unit for acid titration). The samples were prefiltered through 0.45 µm polyvinylidene fluoride filters and the estimated precision based on the CRMs (n = 108) is ±1.5 µmol kg^{-1}.

We measured DIC on hydrocast samples within ∼ 4 h of collection without filtration. We acidified 1.25 mL of the sample using a custom built injection system coupled to an infrared gas analyzer (LI-COR LI7000). As described by Long et al. (2011), the infrared absorption signal vs. time is integrated for each stripped gas sample to yield a total mass of CO_2. Samples were run in triplicate or greater and were calibrated using CRMs between every 3–4 unknowns. Micro-bubbles regularly appeared within injected samples due to sample warming between acquisition and DIC analysis. Each integration curve was visually inspected and integration curves that exhibited evidence for bubbles were rejected. The estimated precision based upon unknowns (> 3500 runs) and CRM replicates (n = 855) for cruise NPB-1302 is ±3 µmol kg^{-1}.

BGD
12, 8429–8465, 2015

3.2 Carbon system calculations and crosschecks

We calculate Ω and DIC (hereafter called DIC_{calc}) with CO2SYS for MATLAB (Lewis and Wallace, 1998; van Heuven et al., 2009) with TA, pCO_2, SST, and salinity as input variables. Calculations are only conducted for pCO_2 measured within 3 min of the TA measurement ($n = 1034$), the average cycle time for the automated pCO_2 measurements. We use the equilibrium constants of Mehrback et al. (1973) as refit by Dickson and Millero (1987) since previous studies have found that they are the optimal choice, including for Antarctic waters (e.g. McNeil et al., 2007; Lee et al., 2000; Millero et al., 2002). For the hydrocast data, we calculate Ω using TA, DIC, temperature, and salinity as input variables.

As a means of internal quality control, we use the initial pH reading from the TA titration as a third carbon system parameter to crosscheck the accuracy of our Ω_{Ar} estimates. In terms of consistency, Ω_{Ar} calculated using TA and pCO_2 is 0.02 ± 0.07 greater than Ω_{Ar} calculated using TA and pH. In addition, DIC_{calc} using TA and pCO_2 is $2 \pm 7\,\mu mol\,kg^{-1}$ lower than DIC_{calc} using TA and pH. Finally, measured pCO_2 is $4 \pm 14\,\mu atm$ lower than pCO_2 calculated from TA and pH. These strong consistencies suggest that our pCO_2 and TA measurements are accurate. Our surface TA and DIC_{calc} measurements vs. latitude for the Southern Ocean are within the ranges of other studies (Ma[illegible]dotter Björk et al., 2014; McNeil et al., 2007; Metzl et al., 2006).

We compare the TA measurements from the surface hydrocasts (< 5 m deep) to the underway TA measurements made while the ship was still on station within ~ 15 min of when the surface samples were collected. The underway values are $3 \pm 5\,\mu mol\,kg^{-1}$ higher than the hydrocast TA values.

3.3 Ross Sea and Southern Ocean calculations

The Ω_{Ar} of surface waters in the Ross Sea increases during the austral summer months (McNeil et al., 2010). We use DIC, TA, SST, and salinity to determine the controls on the seasonal cycle of surface water Ω_{Ar}. We normalize DIC and TA to a salinity

BGD
12, 8429–8465, 2015

of 34.5, the average salinity of the Ross Sea (hereafter called sDIC and sTA). Due to the deep convective mixing during the winter, we use the average sDIC and sTA concentrations of hydrocast samples collected from 200–400 m to determine winter water values (sDIC = 2221 ± 5 µmol kg^{-1}, sTA = 2338 ± 3 µmol kg^{-1}). While sDIC and sTA concentrations below 200 m are influenced by carbon export particularly in the summer and early autumn, observations show that sDIC and sTA concentrations are relatively uniform below 200 m across space and a given season (Table 1).

Following Hauri et al. (2013), the change in Ω_{Ar} of surface hydrocast samples (upper 10 m) from winter conditions can be expressed as:

$$\Delta\Omega_{Ar} = \frac{\partial\Omega}{\partial \mathrm{DIC}}\Delta\,\mathrm{sDIC} + \frac{\partial\Omega}{\partial \mathrm{TA}}\Delta\,\mathrm{sTA} + \frac{\partial\Omega}{\partial T}\Delta T + \Delta S_{\Omega} + \text{ Residuals} \quad (2)$$

where

$$\Delta S_{\Omega} = \frac{\partial\Omega}{\partial S}\Delta S + \frac{\partial\Omega}{\partial \mathrm{DIC}}\Delta\,\mathrm{DIC}^{S} + \frac{\partial\Omega}{\partial \mathrm{TA}}\Delta\,\mathrm{TA}^{S} \quad (3)$$

Δ sDIC and Δ sTA are the difference in sDIC and sTA for each sample from the winter value. The term ΔT is calculated using a winter SST of −1.89 °C (per Sweeney, 2003). ΔS_{Ω} represents the total contribution of salinity changes to $\Delta\Omega_{Ar}$.

Since salinity between 200 to 400 m is variable across the Ross Sea (Orsi and Wiederwohl, 2009), ΔS is calculated as the difference between the salinity of a surface sample and the average salinity for samples from that station that are between 200–400 m.

Δ DIC^{S} and Δ TA^{S} represent changes to DIC and TA due to dilution/concentration from freshwater input and sea-ice processes:

$$\Delta\,\mathrm{DIC}^{S} = [\mathrm{DIC}_{200\text{–}400} \cdot (\mathrm{Salinity}_{\text{surface sample}}/\mathrm{Salinity}_{200\text{–}400})] - \mathrm{DIC}_{200\text{–}400} \quad (4)$$

$$\Delta\,\mathrm{TA}^{S} = [\mathrm{TA}_{200\text{–}400} \cdot (\mathrm{Salinity}_{\text{surface sample}}/\mathrm{Salinity}_{200\text{–}400})] - \mathrm{TA}_{200\text{–}400} \quad (5)$$

$\mathrm{DIC}_{200\text{–}400}$, $\mathrm{TA}_{200\text{–}400}$, and $\mathrm{Salinity}_{200\text{–}400}$ are the average values for samples collected from 200–400 m calculated at each station.

BGD
12, 8429–8465, 2015

The partial derivatives quantify the change in Ω_{Ar} per unit change in DIC, TA, temperature, and salinity respectively. To determine the partial derivatives, we calculate Ω_{Ar} for all hydrocast samples within the upper 10 m using DIC, TA, temperature, and salinity as input parameters. We recalculate Ω_{Ar} after independently increasing DIC, TA, temperature, and salinity by one unit. The partial derivatives are the average difference between the initial Ω_{Ar} and the recalculated Ω_{Ar}.

We use the same equations to evaluate the relative importance of DIC, TA, temperature, and salinity on the variability of Ω_{Ar} from 75 to 55° S. For the Δ terms, we calculate the change in sDIC, sTA, temperature, and salinity from the mean of the first 6 underway measurements at 75° S. For Eqs. (4) and (5), instead of using DIC, TA, and salinity values from 200–400 m, we use the mean of the first 6 underway measurements at 75° S.

4 Results and discussion

4.1 Ω in the Ross Sea

We define the area west of 171° E as the western region and the area between 171 and 180° E as the central region. This demarcation is similar to regions defined by Sweeney et al. (2000a) and roughly traces the western boundary between sea ice and open water when the Ross Sea polynya is opening during austral spring (Fig. 2a).

Surface water salinity is lower in the western region (33.79 ± 0.27) than the central region (34.11 ± 0.10) (Fig. 2b). While sea ice advects northwards in the central region as the Ross Sea polynya forms, in the western region much of the sea ice melts in place lowering the surface salinity and increasing stratification. Monthly Aqua MODIS chlorophyll concentration data shows that the highest chlorophyll concentrations during February 2013 are in the western region (Fig. 2c). Arrigo et al. (1999) also observed that diatom blooms in the highly stratified western region peak during the early autumn ~ 6 weeks after the main *Phaeocystis antarctica* bloom in the central Ross Sea.

BGD
12, 8429–8465, 2015

Surface TA values range from 2268 to 2346 µmol kg^{-1} (mean = 2314 ± 16 µmol kg^{-1}). Since TA strongly covaries with salinity (R^2 = 0.86, residual ±6 µmol kg^{-1}), the lowest TA values are located in the western region. Values of sTA range from 2336 to 2386 µmol kg^{-1} (mean = 2360 ± 7 µmol kg^{-1}) and are influenced by calcification/dissolution as well as phytoplankton photosynthesis since one unit of nitrate drawdown increases TA by one unit (Brewer and Goldman, 1978) (Fig. 2d).

Surface pCO_2 values range from 162 to 354 µatm (Fig. 2e). Surface pCO_2 values are lower in the western region (238 ± 34 µatm) compared to the central region (319 ± 16 µatm) due to greater phytoplankton photosynthesis in the west. Surface Ω_{Ar} values range from 1.40 to 2.42 and Ω_{Ca} ranges from 2.24 to 3.89 (Fig. 2f). The highest Ω_{Ar} values are in the western region (1.94±0.18, Ω_{Ca} = 3.09±0.30) compared to the central region (1.58 ± 0.09, Ω_{Ca} = 2.52 ± 0.14). Greater phytoplankton photosynthesis in the western region increases Ω by both decreasing DIC and increasing TA.

Spatial and temporal variations in surface water Ω_{Ar} are mainly controlled by sDIC in the Ross Sea (Fig. 3). The concentration of sDIC decreased by 58 ± 20 µmol kg^{-1} from a winter value, causing Ω_{Ar} to increase by 0.5 ± 0.2. In addition, sTA increased by 11 ± 7 µmol kg^{-1} during the preceding summer months, causing Ω_{Ar} to increase by 0.1 ± 0.1. Although there was a significant reduction in salinity compared to winter values (0.7±0.3), Ω_{Ar} only decreased by ~ 0.01 due to this freshening since both DIC and TA concentrations were reduced. Lastly, the effect of temperature on Ω_{Ar} was negligible since the Ross Sea only experiences a 2 °C seasonal change in SSTs (Sweeney, 2003).

Two processes can reduce sDIC: calcification and phytoplankton photosynthesis. To evaluate the importance of calcification, we use time dependent changes in potential alkalinity (pTA, defined as sNitrate + sTA) from a winter value (2367±3 µmol kg^{-1}, defined as average value for all samples between 200–400 m). While TA will increase during photosynthesis due to nitrate drawdown, pTA will be conserved. Therefore, changes in pTA can be attributed to calcification and dissolution. The average ΔpTA from a winter concentration is negligible (0 ± 5 µmol kg^{-1}); therefore, calcification appears to be

BGD
12, 8429–8465, 2015

insignificant and the increase in sTA from winter conditions is largely driven by nitrate drawdown during photosynthesis. Earlier studies found that calcification contributed to only ∼ 5 % of the total seasonal DIC drawdown (Sweeney et al., 2000a; Bates et al., 1998). Therefore, we argue that photosynthesis exerts the dominant control on sDIC, sTA, and Ω_{Ar}. While the highest Ω_{Ar} value that we observed was 2.4, values up to ∼ 4 have been observed during December–January (McNeil et al., 2010). By the time we arrived in the Ross Sea, surface sDIC concentrations would have already increased relative to the summer due to enhanced air–sea CO_2 fluxes (Arrigo and Van Dijken, 2007), deepening of the mixed layer (Sweeney, 2003), and remineralization of organic carbon (Sweeney et al., 2000b).

Mattsdotter Björk et al. (2014) also argue that phytoplankton photosynthesis is the major control on surface water Ω_{Ar} variability between the Ross Sea and the Antarctic Peninsula based upon the covariance of Ω_{Ar} and chlorophyll *a*. The largest contributor to seasonal Ω_{Ar} change in the Chukchi Sea in the Arctic is also phytoplankton photosynthesis (Bates et al., 2013). However, unlike the Ross Sea, in parts of the Arctic sea ice melt and river runoff leads to significant reductions in Ω_{Ar} (Chierici and Fransson, 2009; Yamamoto et al., 2009; Robbins et al., 2013).

4.2 Ω in the Southern Ocean

The spatial changes in Ω_{Ar}, SST, pCO_2, and particulate organic matter (POC) between 75 and 55° S are shown in Fig. 4. The lowest Ω_{Ar} value is 1.25 (Ω_{Ca} = 2.00) at 75° S, corresponding with the highest pCO_2 of ∼ 396 µatm. Ω_{Ar} increases along the transect to reach a maximum of 1.93 (Ω_{Ca} = 3.04) at 55° S. The rate of increase is not always linear. Changes in Ω_{Ar} sometimes correspond to drops in pCO_2. For instance, between 74 and 73° S, Ω_{Ar} first increases and then decreases by ∼ 0.1. This corresponds with a 40 µatm drop and then rise in pCO_2. Given that SST is constant, this localized increase in Ω_{Ar} is likely due to phytoplankton photosynthesis. This region may be along the Antarctic Slope Front that is known for higher biological activity (Jacobs, 1991). There is another step in Ω_{Ar} from ∼ 1.4 to ∼ 1.5 between 67.5 and 67° S. This step also

BGD
12, 8429–8465, 2015

corresponds with a decrease in pCO_2 from ~370 to ~340 µatm, likely due to phytoplankton photosynthesis. Elevated POC concentrations and lower pCO_2 values around the PF indicate enhanced phytoplankton photosynthesis. Ruben (2003) also found that pCO_2 is reduced south of the PF (170° W) due to primary production.

We quantify the contribution of changing sDIC (calculated from TA and pCO_2), sTA, SST, and salinity to changing Ω_{Ar} along the transect (Fig. 5a). The dominant control is declining $sDIC_{calc}$ from ~2240 to ~2140 µmol kg^{-1} between 75 and 55° S, which causes Ω_{Ar} to increase by 0.87 if sTA, SST, and salinity are held constant. Declining sTA from ~2340 to ~2310 µmol kg^{-1} partially counters the influence of $sDIC_{calc}$ and reduces Ω_{Ar} by 0.28. The influences of SST and salinity on Ω_{Ar} are minimal.

Ω_{Ar} variability is driven almost entirely by changes in $sDIC_{calc}$ from 75° S to the PF. Between the PF and SAF, variability in Ω_{Ar} is influenced by the opposing effects of $sDIC_{calc}$ and sTA. The $TA : DIC_{calc}$ ratio and Ω_{Ar} are constant between the PF and 60° S since both $sDIC_{calc}$ and sTA decrease at the same rate. Between 60° S and the SAF, Ω_{Ar} increases since $sDIC_{calc}$ declines faster than sTA (Fig. 5b). North of the SAF, Ω_{Ar} variability is again driven by $sDIC_{calc}$: Ω_{Ar} increases due to a decrease in $sDIC_{calc}$ while sTA remains constant.

The concentration of $sDIC_{calc}$ is highest south of the PF due to upwelling of CDW (Fig. 6a). To evaluate the properties of CDW, we use data from the 2011 Repeat Hydrography Cruise SO4P, which is part of the U.S. Climate Variability and Predictability (CLIVAR) program (Swift and Orsi, 2012) (available at http://www.clivar.org/resources/data/hydrographic). We only use data from hydrocasts located between 168° E–73° W where the bottom depth is > 1000 m (Fig. 1b). We reject the data from hydrocast 46(B) where the deep DIC data below 200 m is ~30 µmol kg^{-1} higher than the rest of the stations. Following Sweeney (2003), CDW is defined as centered on the level of maximum temperature below 150 m.

From this CLIVAR dataset, CDW has a sDIC value of 2243 ± 3 µmol kg^{-1}. Between 75 and 74° S, $sDIC_{calc}$ concentration of surface water is also 2243 ± 5 µmol kg^{-1}, indicating little modification to CDW and consistent with the observation that this region

BGD
12, 8429–8465, 2015

was covered by sea ice even during the summer of 2013. At 74° S $sDIC_{calc}$ drops to ~ 2220 µmol kg^{-1} and at 67.5° S $sDIC_{calc}$ drops to ~ 2200 µmol kg^{-1}. The main driver of this 40 µmol kg^{-1} decrease in $sDIC_{calc}$ between Antarctica and the PF is likely photosynthesis. Ruben et al. (1998) also observed a 30–50 µmol kg^{-1} decrease in sDIC at 67° S in Pacific Antarctic waters between winter and summer that they attribute to primary productivity.

$sDIC_{calc}$ continues to drop from ~ 2220 µmol kg^{-1} at the PF to ~ 2140 µmol kg^{-1} at 55° S, consistent with surface DIC measurements between 70 and 40° S compiled by McNeil et al. (2007). There are multiple factors likely responsible for this decrease in $sDIC_{calc}$. Both satellite (Arrigo et al., 2008) and in situ measurements (Reuer et al., 2007) show that annual primary productivity increases from south to north in the Southern Ocean. In addition, surface waters north of the PF advect northwards and accumulate a sDIC deficit. Finally, warmer water holds less DIC while in equilibrium with the atmosphere. There is little net air–sea CO_2 flux between 75 and 55° S (except for net efflux at 60° S) since warming and increased biological production compensate each other (Takahashi et al., 2012).

The concentration of sTA is also highest south of the PF due to upwelling of CDW. Based off the CLIVAR dataset, the sTA of CDW is 2334 ± 3 µmol kg^{-1}. Surface water between 74° S and the PF has a relatively constant sTA concentration of ~ 2340 µmol kg^{-1}, slightly higher than its CDW source (Fig. 6b). Nitrate drawdown during photosynthesis may explain the elevated sTA. Between 75 and 74° S, sTA exceeds 2360 µmol kg^{-1}. One possible explanation is that ikaite ($CaCO_3 \times 6H_2O$), a mineral that has been observed directly and indirectly to precipitate in Antarctic sea ice (Dieckmann et al., 2008; Fransson et al., 2011), dissolved into surface waters during the summer causing sTA concentrations to increase. Between the PF and SAF, sTA drops to 2310 µmol kg^{-1} where the concentrations level off. This drop appears to be in part due to the mixing of two end member water masses, AASW south of the PF and subtropical water north of the SAF. The decreasing sTA is consistent with the suggestion

BGD
12, 8429–8465, 2015

of Millero et al. (1998) that a negative linear relationship between sTA and SST is due to colder water being indicative of greater upwelling of TA rich water.

This dataset supports the argument that increased upwelling of CDW from strengthening westerly winds will increase OA in the Southern Ocean (Lenton et al., 2009). While the TA : DIC ratio for CDW is 1.040±0.002, the TA : DIC_{calc} ratio for surface waters between 75° S and the PF ranges from 1.046 to 1.064 (Fig. 5b). Therefore increased upwelling will lower the TA : DIC ratio and cause Ω_{Ar} to decrease.

4.3 Estimate of wintertime surface Ω_{Ar} values in the Ross Sea

Efforts to predict winter Ω_{Ar} undersaturation in the Ross Sea are complicated by the complete lack of carbon system measurements from the winter months in the Ross Sea.

McNeil et al. (2010) estimated winter surface water Ω_{Ar} by using the lowest observed Ω_{Ar} value from early spring when the Ross Sea is still covered by sea ice. They used mid October and early November carbon system measurements from the Joint Global Ocean Flux Study (JGOFS) (Sweeney et al., 2000b). Although sea ice algae productivity peaks in November, their impact on water column DIC concentrations is likely to be negligible (Saenz and Arrigo, 2014). McNeil et al. (2010) found that early spring surface water Ω_{Ar} was ∼ 1.2. There was a single Ω_{Ar} value < 1.1 that they used as an initial condition along with the IPCC US92a scenario to predict that surface waters of the Ross Sea could begin to experience seasonally undersaturated conditions with respect to aragonite as early as 2015 if full equilibrium with rising atmospheric CO_2 is achieved. Based on a three-dimensional Coupled Ice, Atmosphere, and Ocean model (Arrigo et al., 2003; Tagliabue and Arrigo, 2005), McNeil et al. (2010) argued that only 35 % of the atmospheric CO_2 signal equilibrates with Ross Sea surface waters due to sea ice, upwelling of CDW, and short residence times, thereby delaying the onset of aragonite undersaturation until 2045. Decadal wintertime surface carbon system measurements do not exist to directly validate this disequilibrium assumption. In addition, McNeil et al. (2010) would inaccurately predict when the Ross Sea would become un-

BGD
12, 8429–8465, 2015

dersaturated with respect to aragonite if the minimum wintertime surface Ω_{Ar} value used was low due to measurement error.

To independently calculate Ω_{Ar} from early spring surface waters, we use the LDEO pCO_2 measurements from November 1994, 1997, 2005, and 2006 that are from the Ross Shelf (defined by the 1000 m isopleth) and are south of 74° S (Fig. 7a). The earliest pCO_2 measurements are from 16 November 1994, 17 November 1997, 6 November 2005, and 13 November 2006 when much of the Ross Sea is still covered in sea ice. The earliest measurements from 2005/06 are more likely to represent winter conditions since they are from 74° S as the NBP entered the Ross Sea. Conversely, the earliest measurements from 1994/97 are from the 76.5° S line, close to where the Ross Sea polynya opens up from.

We calculate wintertime TA in the Ross Sea by establishing a salinity-TA relationship using data from Bates et al. (1998), Sweeney et al. (2000b), and our own hydrocast TA measurements from the upper 10 m (Fig. 7b). Since one unit of nitrate drawdown increases TA by one unit, the TA measurements are adjusted to winter nitrate concentrations of 29 µmol kg^{-1} (the mean nitrate concentration between 200–400 m from our cruise). The relationship between TA and salinity is consistent among these independent datasets and the standard deviation of the residuals for TA is ±5 µmol kg^{-1}.

We calculate historical Ω_{Ar} using historical pCO_2 measurements, TA calculated from salinity, SST, and salinity. Phosphate and silicate are set to the winter values of 2.1 and 79 µmol kg^{-1} respectively. The thermosalinograph (TSG) salinity data from the historical pCO_2 measurements appears reasonable and is uncalibrated. While the largest offset in TSG salinity compared with Autosal measurements is 0.3, such error is not typical. For instance, on our cruise the difference between TSG and Autosal measurements is less than 0.02. To test the possible impact of a poor salinity calibration, we recalculate Ω_{Ar} for all pCO_2 measurements after increasing salinity by 0.3. TA calculated from the observed TA-salinity relationship increases by ~ 21 µmol kg^{-1} and Ω_{Ar} increases by 0.024 ± 0.003.

BGD
12, 8429–8465, 2015

The lowest Ω_{Ar} measurements are 1.24 in 1994, 1.25 in 1997, 1.22 in 2005, and 1.20 in 2006 (Fig. 7c). Although Ω_{Ar} declines from 1994 to 2006, we have low confidence in any trend due to spatial–temporal sampling biases. The lowest Ω_{Ar} values are consistently between 1.2 and 1.3 as the ship crossed sea ice covered regions and open water that had experienced DIC drawdown. With the exception of a single measurement, the lowest 1996/97 Ω_{Ar} values from McNeil et al. (2010) are also ~ 1.2. The similarity between the Ω_{Ar} values reported by McNeil et al. (2010) from 1996/97 and our 2005/06 values is consistent with their delayed acidification hypothesis.

A simple calculation also suggests that wintertime Ω_{Ar} values may be closer to 1.2 than 1.1. If salinity is 34.5, approximately the mean salinity of the water column, TA would be 2339 µmol kg^{-1} based on the observed TA-salinity linear relationship. Sweeney (2003) estimates winter pCO_2 values of ~ 425 µatm based on deep pCO_2 measurements made during early spring. Setting salinity to 34.5, TA to 2339 µmol kg^{-1}, pCO_2 to 425 µatm, temperature to −1.89, silicate to 79 µmol kg^{-1}, and phosphate to 2.1 µmol kg^{-1} yields a Ω_{Ar} value of 1.22.

Although pCO_2 measurements of surface waters colder than −1.75 °C south of 60° S typically reach ~ 410 µatm by September, Takahashi et al. (2009) present a few measurements of ~ 450 µatm. Even if pCO_2 reaches 450 µatm during winter in the Ross Sea, Ω_{Ar} would be 1.16 (with salinity at 34.5 and TA at 2339 µmol kg^{-1}). In order to obtain Ω_{Ar} of 1.1, pCO_2 would need to be ~ 480 µatm, a value that appears unreasonably high given the available datasets from the Ross Sea.

McNeil et al. (2010) calculated the Ω_{Ar} of water arriving onto the Ross Shelf following the recipes of Jacobs and Fairbanks (1985): 50 % CDW, 25 % Tmin water (minimum temperature in upper 100 m), and 25 % AASW. To calculate the Ω_{Ar} of these three source water masses, they used hydrocast temperature, salinity, and DIC data collected during the austral winter of 1994 from north of the Ross Shelf as described in Sweeney (2003). They calculated that the average Ω_{Ar} of incoming water would be 1.08.

BGD
12, 8429–8465, 2015

We independently calculate Ω_{Ar} of incoming water using the 2011 CLIVAR hydrocast data from north of the Ross Shelf between 168° E–73° W as described earlier (Fig. 1b). The Ω_{Ar} of water in the upper 100 m (AASW and Tmin) from the CLIVAR dataset is 1.36 ± 0.13 and the Ω_{Ar} of CDW (maximum temperature below 150 m) is 1.18 ± 0.03 (Fig. 7d). Even if 100 % of the incoming water onto the Ross Shelf is CDW, the Ω_{Ar} of this incoming water would be significantly greater than 1.08. While most properties of CDW are similar between the 2011 CLIVAR data and the 1994 data used by McNeil et al. (2010), the TA of CDW from the CLIVAR dataset is 18 µmol kg^{-1} higher (Table 2).

Another approach to estimate the Ω_{Ar} of winter surface waters is to use the properties of water below 200 m. For the TRACERS data, sTA below 200 m is 2338 ± 2 µmol kg^{-1}. For the JGOFS autumn cruise (NBP 97-3) sTA below 200 m is 2339 ± 2 µmol kg^{-1}. Using the CLIVAR dataset, sTA of CDW from off the Ross Shelf is 2334 ± 3 µmol kg^{-1}. This consistency between independent datasets suggests that we can accurately estimate winter TA in the Ross Sea.

The range in sDIC below 200 m is much greater than that for sTA (Table 2). The lowest value is 2220 ± 5 µmol kg^{-1} from our cruise and the highest is 2237 ± 3 µmol kg^{-1} from the summer JGOFS cruise (NBP 97-01). This range in sDIC concentrations below 200 m is not surprising given that sDIC concentrations vary across the input water masses. In addition, sDIC concentrations below 200 m will be influenced by carbon export particularly in summer and early autumn and over multiple seasons' air to sea flux of CO_2.

Assuming that deep water concentrations of TA and DIC are relatively unmodified following wintertime deep convective mixing, we estimate the Ω_{Ar} of winter surface water by setting TA to 2338 µmol kg^{-1}, salinity to 34.5, temperature to −1.89 °C, phosphate to 2.1 µmol kg^{-1}, and silicate to 79 µmol kg^{-1}. If DIC concentrations are 2220 µmol kg^{-1}, Ω_{Ar} would be 1.37. If sDIC concentrations are 2237 µmol kg^{-1}, Ω_{Ar} would be 1.24 and pCO_2 would be 417 µatm. These results are consistent with a study by Matson et al. (2014) where early spring Ω_{Ar} at 20 m depth calculated using pH and salinity derived TA was 1.2–1.3 from Hut Point (bottom depth > 200 m) and Cape Evans (bot-

BGD
12, 8429–8465, 2015

tom depth < 30 m) in McMurdo Sound. The lowest measured winter surface Ω_{Ar} values were also ~ 1.2 during 1993–1995 in Prydz Bay (McNeil et al., 2011).

Hofmann et al. (2015) report Ω_{Ar} at 18 m depth (bottom depth < 30 m) at two coastal sites in McMurdo Sound, the Jetty and Cape Evans, for December–May and November–June respectively using pH and salinity derived TA as input variables. The lowest Ω_{Ar} observations were from May at both sites and were 1.22 and 0.96 at the Jetty and Cape Evans. The maximum calculated pCO_2 was 559 at Cape Evans. The low Ω_{Ar} and high calculated pCO_2 values measured by Hofmann et al. (2015) may represent differences between coastal and open ocean systems – there may be a coastal amplification signal when sinking organic matter hits a shallow bed. Another possibility is that their carbon system time series, particularly at Cape Evans, is inaccurate. After conditioning and calibrating their pH measurements using discrete water samples, for logistical reasons Hofmann et al. (2015) could not collect additional validation samples during deployment or measure multiple carbon system parameters for cross-check. Although the SeaFET pH sensors that they used are generally stable, they can drift (Bresnahan et al., 2014). Hofmann et al. (2015) have no means to assess possible pH sensor drift.

Following McNeil et al. (2010) and a Representative Concentration Pathway (RCP8.5) scenario (Meinshausen et al., 2011), we use the lowest Ω_{Ar} values from 2006 (Ω_{Ar} = 1.20, pCO_2 = 428 µatm, TA = 2328 µmol kg^{-1}, salinity = 34.33, SST = −1.87 °C, phosphate = 2.1 µmol kg^{-1}, silicate = 79 µmol kg^{-1}) to assess when the Ross Sea could become corrosive to aragonite. While shelf water salinity in the Ross Sea has declined by 0.03 decade^{-1} from 1958 to 2008 (Jacobs and Giulivi, 2010), we show that such rates of change will have inconsequential effects on Ω_{Ar}. For equilibrium conditions, surface waters in the Ross Sea would become corrosive to aragonite by 2040 (2092 for calcite). In the disequilibrium scenario (McNeil et al., 2010), surface aragonite undersaturation state would occur by 2071 (2185 for calcite).

In conclusion, we argue that it is unlikely that the Ross Sea actually experienced winter surface Ω_{Ar} values of ~ 1.1 during 1996 and that a Ω_{Ar} value of ~ 1.2 may

BGD
12, 8429–8465, 2015

more accurately represent current winter conditions. Since predictions are sensitive to current surface wintertime Ω_{Ar} values as well as the extent of disequilibrium, highly accurate over-determined carbon system measurements from the winter are crucial.

The Supplement related to this article is available online at doi:10.5194/bgd-12-8429-2015-supplement.

Acknowledgements. This work was supported by the U.S. NSF (OPP-1142044 to R. B. Dunbar) and a NSF Graduate Research Fellowship grant (DGE-114747 to H. B. DeJong). We thank the captain and crew of the R/V *Nathaniel B. Palmer*. We thank S. Bercovici for the nitrate data.

References

Accornero, A., Manno, C., Esposito, F., and Gambi, M. C.: The vertical flux of particulate matter in the polynya of Terra Nova Bay. Part II. Biological components, Antarct. Sci., 15, 175–188, doi:10.1017/S0954102003001214, 2003.

Andersson, A. J., Mackenzie, F. T., and Gattuso, J.-P.: Effects of ocean acidification on benthic processes, organisms, and ecosystems, in: Ocean Acidification, edited by: Gattuso, J.-P. and Hanson, L., Oxford University Press, New York, 122–153, 2011.

Archer, D., Eby, M., Brovkin, V., Ridgwell, A., Cao, L., Mikolajewicz, U., Caldeira, K., Matsumoto, K., Munhoven, G., Montenegro, A., and Tokos, K.: Atmospheric lifetime of fossil fuel carbon dioxide, Annu. Rev. Earth Pl. Sc., 37, 117–134, doi:10.1146/annurev.earth.031208.100206, 2009.

Arrigo, K. R. and McClain, C. R.: Spring phytoplankton production in the western Ross Sea, Science, 266, 261–263, doi:10.1126/science.266.5183.261, 1994.

Arrigo, K. R. and van Dijken, G. L.: Phytoplankton dynamics within 37 Antarctic coastal polynya systems, J. Geophys. Res., 108, 3271, doi:10.1029/2002JC001739, 2003.

Arrigo, K. R. and Van Dijken, G. L.: Interannual variation in air–sea CO_2 flux in the Ross Sea, Antarctica: a model analysis, J. Geophys. Res., 112, 1–16, doi:10.1029/2006JC003492, 2007.

BGD
12, 8429–8465, 2015

Arrigo, K. R., Robinson, D. H., Worthen, D. L., Dunbar, R. B., DiTullio, G. R., VanWoert, M., and Lizotte, M. P.: Phytoplankton community structure and the drawdown of nutrients and CO_2 in the Southern Ocean, Science, 283, 365–367, doi:10.1126/science.283.5400.365, 1999.

Arrigo, K. R., Worthen, D. L., and Robinson, D. H.: A coupled ocean-ecosystem model of the Ross Sea: 2. Iron regulation of phytoplankton taxonomic variability and primary production, J. Geophys. Res., 108, 3231, doi:10.1029/2001JC000856, 2003.

Arrigo, K. R., van Dijken, G. L., and Bushinsky, S.: Primary production in the Southern Ocean, 1997–2006, J. Geophys. Res., 113, C08004, doi:10.1029/2007JC004551, 2008.

Bates, N. R., Hansell, D. A., Carlson, C. A., and Gordon, L. I.: Distribution of CO_2 species, estimates of net community production, and air–sea CO_2 exchange in the Ross Sea polynya, J. Geophys. Res., 103, 2883–2896, doi:10.1029/97jc02473, 1998.

Bates, N. R., Orchowska, M. I., Garley, R., and Mathis, J. T.: Summertime calcium carbonate undersaturation in shelf waters of the western Arctic Ocean – how biological processes exacerbate the impact of ocean acidification, Biogeosciences, 10, 5281–5309, doi:10.5194/bg-10-5281-2013, 2013.

Bednaršek, N., Tarling, G. A., Bakker, D. C. E., Fielding, S., Jones, E. M., Venables, H. J., Ward, P., Kuzirian, A., Lézé, B., Feely, R. A., and Murphy, E. J.: Extensive dissolution of live pteropods in the Southern Ocean, Nat. Geosci., 5, 881–885, doi:10.1038/ngeo1635, 2012.

Bresnahan, P. J., Martz, T. R., Takeshita, Y., Johnson, K. S., and Lashomb, M.: Best practices for autonomous measurement of seawater pH with the Honeywell Durafet, Methods Oceanogr., 9, 1–33, doi:10.1016/j.mio.2014.08.003, 2014.

Brewer, P. G. and Goldman, J. C.: Alkalinity changes generated by phytoplankton growth, Limnol. Oceanogr., 21, 108–117, doi:10.4319/lo.1976.21.1.0108, 1976.

Burling, R. W.: Hydrology of circumpolar waters south of New Zealand, New Zealand Department of Scientific and Industrial Research Bulletin, 143, 66, 1961.

Caldeira, K. and Wickett, M. E.: Oceanography: anthropogenic carbon and ocean pH, Nature, 425, 365, doi:10.1038/425365a, 2003.

Chierici, M. and Fransson, A.: Calcium carbonate saturation in the surface water of the Arctic Ocean: undersaturation in freshwater influenced shelves, Biogeosciences, 6, 2421–2431, doi:10.5194/bg-6-2421-2009, 2009.

Collier, R., Dymond, J., Honjo, S., Manganini, S., Francois, R., and Dunbar, R.: The vertical flux of biogenic and lithogenic material in the Ross Sea: moored sediment trap observations

BGD
12, 8429–8465, 2015

1996–1998, Deep.-Sea Res. Pt. II, 47, 3491–3520, doi:10.1016/S0967-0645(00)00076-X, 2000.
Dickson, A. G.: The carbon dioxide system in seawater: equilibrium chemistry and measurements, in: Guide to Best Practices in Ocean Acidification Reseach and Data Reporting, edited by: Riebesell, U., Fabry, V. J., Hansson, L., and Gattuso, J.-P., Office for Official Publications of the European Communities, Luxembourg, 17–40, 2010.
Dickson, A. G. and Millero, F. J.: A comparison of the equilibrium constants for the dissociation of carbonic acid in seawater media, Deep-Sea Res., 34, 1733–1743, doi:10.1016/0198-0149(87)90021-5, 1987.
Dickson, A. G., Afghan, J. D., and Anderson, G. C.: Reference materials for oceanic CO_2 analysis: a method for the certification of total alkalinity, Mar. Chem., 80, 185–197, doi:10.1016/S0304-4203(02)00133-0, 2003.
Dickson, A. G., Sabine, C. L., and Christian, J. R.: Guide to best practices for ocean CO_2 measurements, PICES Spec. Publ., 3, p. 191, doi:10.1159/000331784, 2007.
Dieckmann, G. S., Nehrke, G., Papadimitriou, S., Göttlicher, J., Steininger, R., Kennedy, H., Wolf-Gladrow, D., and Thomas, D. N.: Calcium carbonate as ikaite crystals in Antarctic sea ice, Geophys. Res. Lett., 35, 35–37, doi:10.1029/2008GL033540, 2008.
Dong, S., Sprintall, J., and Gille, S. T.: Location of the Antarctic Polar Front from AMSR-E satellite sea surface temperature measurements, J. Phys. Oceanogr., 36, 2075–2089, doi:10.1175/JPO2973.1, 2006.
Feely, R., Doney, S., and Cooley, S.: Ocean Acidification: present conditions and future changes in a high-CO_2 world, Oceanography, 22, 36–47, doi:10.5670/oceanog.2009.95, 2009.
Feng, Y., Hare, C. E., Rose, J. M., Handy, S. M., DiTullio, G. R., Lee, P. A., Smith, W. O., Peloquin, J., Tozzi, S., Sun, J., Zhang, Y., Dunbar, R. B., Long, M. C., Sohst, B., Lohan, M., and Hutchins, D. A.: Interactive effects of iron, irradiance and CO_2 on Ross Sea phytoplankton, Deep-Sea Res. Pt. I, 57, 368–383, doi:10.1016/j.dsr.2009.10.013, 2010.
Foster, B. A. and Montgomery, J. C.: Planktivory in benthic nototheniid fish in McMurdo Sound, Antarctica, Environ. Biol. Fishes, 36, 313–318, doi:10.1007/BF00001727, 1993.
Fransson, A., Chierici, M., Yager, P. L., and Smith, W. O.: Antarctic sea ice carbon dioxide system and controls, J. Geophys. Res., 116, C12035, doi:10.1029/2010JC006844, 2011.
Gordon, L. I., Codispoti, L. A., Jennings Jr., J. C., Millero, F. J., Morrison, J. M., and Sweeney, C.: Seasonal evolution of hydrographic properties in the Ross Sea, Antarctica, 1996–1997, Deep-Sea Res. Pt. II, 47, 3095–3117, doi:10.1016/S0967-0645(00)00060-6, 2000.

BGD
12, 8429–8465, 2015

Hauck, J., Arrigo, K. R., Hoppema, M., Van Dijken, G. L., Völker, C., and Wolf-Gladrow, D. A.: Insignificant buffering capacity of Antarctic shelf carbonates, Global Biogeochem. Cy. 27, 11–20, doi:10.1029/2011GB004211, 2013.

Hauri, C., Gruber, N., Vogt, M., Doney, S. C., Feely, R. A., Lachkar, Z., Leinweber, A., McDonnell, A. M. P., Munnich, M., and Plattner, G.-K.: Spatiotemporal variability and long-term trends of ocean acidification in the California Current System, Biogeosciences, 10, 193–216, doi:10.5194/bg-10-193-2013, 2013.

Hofmann, G., Kelley, A. L., Shaw, E. C., Martz, T. R., and Hofmann, G. E.: Near-shore Antarctic pH variability has implications for the design of ocean acidification experiments, Sci. Rep., 5, 9638, doi:10.1038/srep09638, 2015.

Hopkins, T. L.: Midwater food web in McMurdo Sound, Ross Sea, Antarctica, Mar. Biol., 96, 93–106, doi:10.1007/BF00394842, 1987.

Hunt, B. P. V., Pakhomov, E. A., Hosie, G. W., Siegel, V., Ward, P., and Bernard, K.: Pteropods in Southern Ocean ecosystems, Prog. Oceanogr., 78, 193–221, doi:10.1016/j.pocean.2008.06.001, 2008.

IPCC AR5 WG1: Climate Change 2013: The Physical Science Basis. Contribution of Working Group I to the Fifth Assessment Report of the Intergovernmental Panel on Climate Change, Rep., Cambridge, UK and New York, NY, USA, 1535 pp., 2013.

Jacobs, S. S.: On the nature and significance of the Antarctic Slope Front, Mar. Chem., 35, 9–24, doi:10.1016/S0304-4203(09)90005-6, 1991.

Jacobs, S. S. and Giulivi, C. F.: Large multidecadal salinity trends near the Pacific–Antarctic continental margin, J. Climate, 23, 4508–4524, doi:10.1175/2010JCLI3284.1, 2010.

Jacobs, S. S., Fairbanks, R. G., and Horibe, Y.: Origin and evolution of water masses near the Antarctic continental margin: evidence from $H_2^{18}O/H_2^{16}O$ ratios in seawater, in: Oceanography of the Antarctic Continental Shelf, Antarctic Research Series, 43, edited by: Jacobs, S. S., American Geophysical Union, Washington, D.C, 59–85, 1985.

Kawaguchi, S., Ishida, A., King, R., Raymond, B., Waller, N., Constable, A., Nicol, S., Wakita, M., and Ishimatsu, A.: Risk maps for Antarctic krill under projected Southern Ocean acidification, Nature Climate Change, 3, 843–847, doi:10.1038/nclimate1937, 2013.

La Mesa, M., Vacchi, M., and Zunini Sertorio, T.: Feeding plasticity of *Trematomus newnesi* (Pisces, Nototheniidae) in Terra Nova Bay, Ross Sea, in relation to environmental conditions, Polar Biol., 23, 38–45, doi:10.1007/s003000050006, 2000.

BGD
12, 8429–8465, 2015

La Mesa, M., Eastman, J. T., and Vacchi, M.: The role of notothenioid fish in the food web of the Ross Sea shelf waters: a review, Polar Biol., 27, 321–338, doi:10.1007/s00300-004-0599-z, 2004.

Lee, K., Millero, F. J., Byrne, R. H., Feely, R. A., and Wanninkhof, R.: The recommended dissociation constants for carbonic acid in seawater, Geophys. Res. Lett., 27, 229, doi:10.1029/1999GL002345, 2000.

Lenton, A., Codron, F., Bopp, L., Metzl, N., Cadule, P., Tagliabue, A., and Le Sommer, J.: Stratospheric ozone depletion reduces ocean carbon uptake and enhances ocean acidification, Geophys. Res. Lett., 36, L12606, doi:10.1029/2009GL038227, 2009.

Lewis, E. and Wallace, D. W. R.: Program Developed for CO_2 System Calculations ORNL/CDIAC-105, Carbon Dioxide Information Analysis Centre, Oak Ridge National Laboratory, US Department of Energy, Tennessee, 1998.

Long, M. C., Dunbar, R. B., Tortell, P. D., Smith, W. O., Mucciarone, D. A., and Ditullio, G. R.: Vertical structure, seasonal drawdown, and net community production in the Ross Sea, Antarctica, J. Geophys. Res.-Oceans, 116, 1–19, doi:10.1029/2009JC005954, 2011.

Manno, C., Tirelli, V., Accornero, A., and Fonda Umani, S.: Importance of the contribution of *Limacina helicina* faecal pellets to the carbon pump in Terra Nova Bay (Antarctica), J. Plankton Res., 32, 145–152, doi:10.1093/plankt/fbp108, 2010.

Matson, P. G., Washburn, L., Martz, T. R., and Hofmann, G. E.: Abiotic versus biotic drivers of ocean pH variation under fast sea ice in McMurdo Sound, Antarctica, 9, e107239, doi:10.1371/journal.pone.0107239, 2014.

Mattsdotter Björk, M., Fransson, A., Torstensson, A., and Chierici, M.: Ocean acidification state in western Antarctic surface waters: controls and interannual variability, Biogeosciences, 11, 57–73, doi:10.5194/bg-11-57-2014, 2014.

McClintock, J. B., Amsler, M. O., Angus, R. A., Challener, R. C., Schram, J. B., Amsler, C. D., Mah, C. L., Cuce, J., and Baker, B. J.: The Mg–calcite composition of Antarctic echinoderms: important implications for predicting the impacts of ocean acidification, J. Geol., 119, 457–466, doi:10.1086/660890, 2011.

McNeil, B. I. and Matear, R. J.: Southern Ocean acidification: a tipping point at 450-ppm atmospheric CO_2, P. Natl. Acad. Sci. USA, 105, 18860–18864, doi:10.1073/pnas.0806318105, 2008.

BGD
12, 8429–8465, 2015

McNeil, B. I., Metzl, N., Key, R. M., Matear, R. J., and Corbiere, A.: An empirical estimate of the Southern Ocean air–sea CO_2 flux, Global Biogeochem. Cy., 21, GB3011, doi:10.1029/2007GB002991, 2007.
McNeil, B. I., Tagliabue, A., and Sweeney, C.: A multi-decadal delay in the onset of corrosive acidified waters in the Ross Sea of Antarctica due to strong air–sea CO_2 disequilibrium, Geophys. Res. Lett., 37, 1–5, doi:10.1029/2010GL044597, 2010.
McNeil, B. I., Sweeney, C., and Gibson, J. A. E.: Short Note: natural seasonal variability of aragonite saturation state within two Antarctic coastal ocean sites, Antarct. Sci., 23, 411–412, doi:10.1017/S0954102011000204, 2011.
Mehrback, C., Culberson, C. H., Hawley, J. E., and Pytkowicz, R. M.: Measurement of the apparent dissociation constants of carbonic acid in seawater at atmospheric pressure, Limnol. Oceanogr., 18, 897–907, doi:10.4319/lo.1973.18.6.0897, 1973.
Metzl, N., Brunet, C., Jabaud-Jan, A., Poisson, A., and Schauer, B.: Summer and winter air–sea CO_2 fluxes in the Southern Ocean, Deep-Sea Res. Pt. I, 53, 1548–1563, doi:10.1016/j.dsr.2006.07.006, 2006.
Millero, F. J., Pierrot, D., Lee, K., Wanninkhof, R., Feely, R., Sabine, C. L., Key, R. M., and Takahashi, T.: Dissociation constants for carbonic acid determined from field measurements, Deep-Sea Res. Pt. I, 49, 1705–1723, doi:10.1016/S0967-0637(02)00093-6, 2002.
Moy, A. D., Howard, W. R., Bray, S. G., and Trull, T. W.: Reduced calcification in modern Southern Ocean planktonic foraminifera, Nat. Geosci., 2, 276–280, doi:10.1038/ngeo460, 2009.
Mucci, A.: The solubility of calcite and aragonite in seawater at various salinities, temperatures, and one atmosphere total pressure, Am. J. Sci., 283, 780–799, doi:10.2475/ajs.283.7.780, 1983.
Orr, J. C., Fabry, V. J., Aumont, O., Bopp, L., Doney, S. C., Feely, R. A., Gnanadesikan, A., Gruber, N., Ishida, A., Joos, F., Key, R. M., Lindsay, K., Maier-Reimer, E., Matear, R., Monfray, P., Mouchet, A., Najjar, R. G., Plattner, G.-K., Rodgers, K. B., Sabine, C. L., Sarmiento, J. L., Schlitzer, R., Slater, R. D., Totterdell, I. J., Weirig, M.-F., Yamanaka, Y., and Yool, A.: Anthropogenic ocean acidification over the twenty-first century and its impact on calcifying organisms, Nature, 437, 681–686, doi:10.1038/nature04095, 2005.
Orsi, A. H. and Wiederwohl, C. L.: A recount of Ross Sea waters, Deep-Sea Res. Pt. II, 56, 778–795, doi:10.1016/j.dsr2.2008.10.033, 2009.
Petty, A. A., Holland, P. R., and Feltham, D. L.: Sea ice and the ocean mixed layer over the Antarctic shelf seas, The Cryosphere, 8, 761–783, doi:10.5194/tc-8-761-2014, 2014.

BGD
12, 8429–8465, 2015

Reuer, M. K., Barnett, B. A., Bender, M. L., Falkowski, P. G., and Hendricks, M. B.: New estimates of Southern Ocean biological production rates from O_2/Ar ratios and the triple isotope composition of O_2, Deep-Sea Res. Pt. I, 54, 951–974, doi:10.1016/j.dsr.2007.02.007, 2007.
Rintoul, S., Hughes, C., and Olbers, D.: The Antarctic circumpolar current system BT – ocean circulation and climate, in: Ocean Circulation and Climate, 271–301, 2001.
Robbins, L. L., Wynn, J. G., Lisle, J. T., Yates, K. K., Knorr, P. O., Byrne, R. H., Liu, X., Patsavas, M. C., Azetsu-Scott, K., and Takahashi, T.: Baseline monitoring of the western Arctic Ocean estimates 20 % of Canadian basin surface waters are undersaturated with respect to aragonite, PLoS One, 8, e73796, doi:10.1371/journal.pone.0073796, 2013.
Rubin, S. I.: Carbon and nutrient cycling in the upper water column across the Polar Frontal Zone and Antarctic Circumpolar Current along 170° W, Global Biogeochem. Cy., 17, 1087, doi:10.1029/2002GB001900, 2003.
Rubin, S. I., Takahashi, T., Chipman, D. W., and Goddard, J. G.: Primary productivity and nutrient utilization ratios in the pacific sector of the Southern Ocean based on seasonal changes in seawater chemistry, Deep-Sea Res. Pt. I, 45, 1211–1234, doi:10.1016/S0967-0637(98)00021-1, 1998.
Saenz, B. T. and Arrigo, K. R.: Annual primary production in Antarctic sea ice during 2005–2006 from a sea ice state estimate, J. Geophys. Res.-Oceans, 119, 3645–3678, doi:10.1002/2013JC009677, 2014.
Seibel, B. A. and Dierssen, H. M.: Cascading trophic impacts of reduced biomass in the Ross Sea, Antarctica: just the tip of the iceberg?, Biol. Bull., 205, 93–97, 2003.
Sewell, M. A. and Hofmann, G. E.: Antarctic echinoids and climate change: a major impact on the brooding forms, Glob. Change Biol., 17, 734–744, doi:10.1111/j.1365-2486.2010.02288.x, 2011.
Shadwick, E. H., Tilbrook, B., and Williams, G. D.: Carbonate chemistry in the Mertz Polynya (East Antarctica): biological and physical modification of dense water outflows and the export of anthropogenic CO_2, J. Geophys. Res.-Oceans, 119, 1–14, doi:10.1002/2013JC009286, 2014.
Smith, W., Sedwick, P., Arrigo, K., Ainley, D., and Orsi, A.: The Ross Sea in a sea of change, Oceanography, 25, 90–103, doi:10.5670/oceanog.2012.80, 2012.
Smith, W. O. and Gordon, L. I.: Hyperproductivity of the Ross Sea (Antarctica) polynya during austral spring, Geophys. Res. Lett., 24, 233, doi:10.1029/96GL03926, 1997.

BGD
12, 8429–8465, 2015

Spreen, G., Kaleschke, L., and Heygster, G.: Sea ice remote sensing using AMSR-E 89-GHz channels, J. Geophys. Res.-Oceans, 113, C02S03, doi:10.1029/2005JC003384, 2008.

Sweeney, C.: The annual cycle of surface water CO_2 and O_2 in the Ross Sea?: a model for gas exchange on the continental shelves of Antarctica, in: Biogeochemistry of the Ross Sea, 295–310, 2003.

Sweeney, C., Hansell, D. A., Carlson, C. A., Codispoti, L. A., Gordon, L. I., Marra, J., Millero, F. J., Smith, W. O., and Takahashi, T.: Biogeochemical regimes, net community production and carbon export in the Ross Sea, Antarctica, Deep-Sea Res. Pt. II, 47, 3369–3394, doi:10.1016/S0967-0645(00)00072-2, 2000a.

Sweeney, C., Smith, W. O., Hales, B., Bidigare, R. R., Carlson, C. A., Codispoti, L. A., Gordon, L. I., Hansell, D. A., Millero, F. J., Park, M. O., and Takahashi, T.: Nutrient and carbon removal ratios and fluxes in the Ross Sea, Antarctica, Deep-Sea Res. Pt. II, 47, 3395–3421, doi:10.1016/S0967-0645(00)00073-4, 2000b.

Swift, J. H. and Orsi, A. H.: Sixty-four days of hydrography and storms: RVIB Nathaniel B. Palmer's 2011 SO4P Cruise, Oceanography, 25, 54–55, doi:10.5670/oceanog.2012.74, 2012.

Tagliabue, A. and Arrigo, K. R.: Iron in the Ross Sea: 1. Impact on CO_2 fluxes via variation in phytoplankton functional group and non-Redfield stoichiometry, J. Geophys. Res.-Oceans, 110, 1–15, doi:10.1029/2004JC002531, 2005.

Takahashi, T., Sutherland, S. C., Wanninkhof, R., Sweeney, C., Feely, R. A., Chipman, D. W., Hales, B., Friederich, G., Chavez, F., Sabine, C., Watson, A., Bakker, D. C. E., Schuster, U., Metzl, N., Yoshikawa-Inoue, H., Ishii, M., Midorikawa, T., Nojiri, Y., Körtzinger, A., Steinhoff, T., Hoppema, M., Olafsson, J., Arnarson, T. S., Tilbrook, B., Johannessen, T., Olsen, A., Bellerby, R., Wong, C. S., Delille, B., Bates, N. R., and de Baar, H. J. W.: Climatological mean and decadal change in surface ocean pCO_2, and net sea–air CO_2 flux over the global oceans, Deep-Sea Res. Pt. II, 56, 554–577, doi:10.1016/j.dsr2.2008.12.009, 2009.

Tortell, P. D., Payne, C. D., Li, Y., Trimborn, S., Rost, B., Smith, W. O., Riesselman, C., Dunbar, R. B., Sedwick, P., and DiTullio, G. R.: CO_2 sensitivity of Southern Ocean phytoplankton, Geophys. Res. Lett., 35, L04605, doi:10.1029/2007GL032583, 2008.

van Heuven, S., Pierrot, D., Rae, J. W. B., Lewis, E., and Wallace, D. W. R.: MATLAB program developed for CO_2 system calculations, ORNL/CDIAC-105b, Carbon Dioxide Information Analysis Center, Oak Ridge National Laboratory, US Department of Energy, Oak Ridge, Tennessee, 2011.

BGD
12, 8429–8465, 2015

Yamamoto-Kawai, M., McLaughlin, F. A., Carmack, E. C., Nishino, S., and Shimada, K.: Aragonite undersaturation in the Arctic Ocean: effects of ocean acidification and sea ice melt, Science, 326, 1098–1100, doi:10.1126/science.1174190, 2009.

BGD
12, 8429–8465, 2015

Table 1. Mean values for sDIC concentrations below 200 m (in μmol kg^{-1}).

Data source	Early Spring	Spring	Summer	Autumn
Sweeney et al. (2000)	2226 ± 3	2233 ± 3	2237 ± 3	2233 ± 5
Long et al. (2011)		2224 ± 5	2225 ± 4	
This paper				2220 ± 5

BGD
12, 8429–8465, 2015

Table 2. Water properties of CDW from McNeil et al. (2010) and CLIVAR.

Data source	Salinity	DIC ($\mu mol\,kg^{-1}$)	TA ($\mu mol\,kg^{-1}$)	PO_4 ($\mu mol\,kg^{-1}$)	SiO_4 ($\mu mol\,kg^{-1}$)	Ω_{Ar}
McNeil et al. (2010)	34.70 ± 0.02	2255 ± 1	2330	2.22 ± 0.0	93.5 ± 1.2	1.01
CLIVAR	34.71 ± 0.02	2257 ± 3	2348 ± 4	2.21 ± 0.0	95.6 ± 6.0	1.18

BGD
12, 8429–8465, 2015

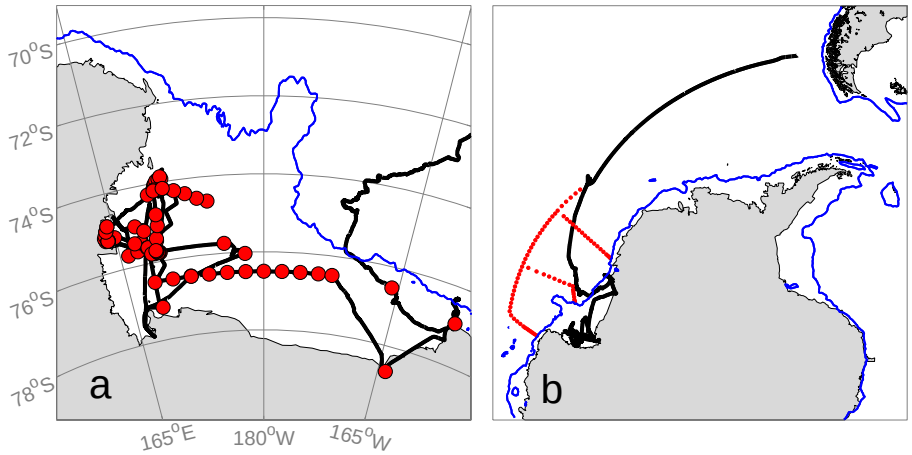

Figure 1. Cruise track (black line) from NBP 13-02. Stations used in this study (red circles) from **(a)** TRACERS (NBP 13-02) and **(b)** CLIVAR (NBP 11-02). Blue line is the 1000 m isobath.

BGD
12, 8429–8465, 2015

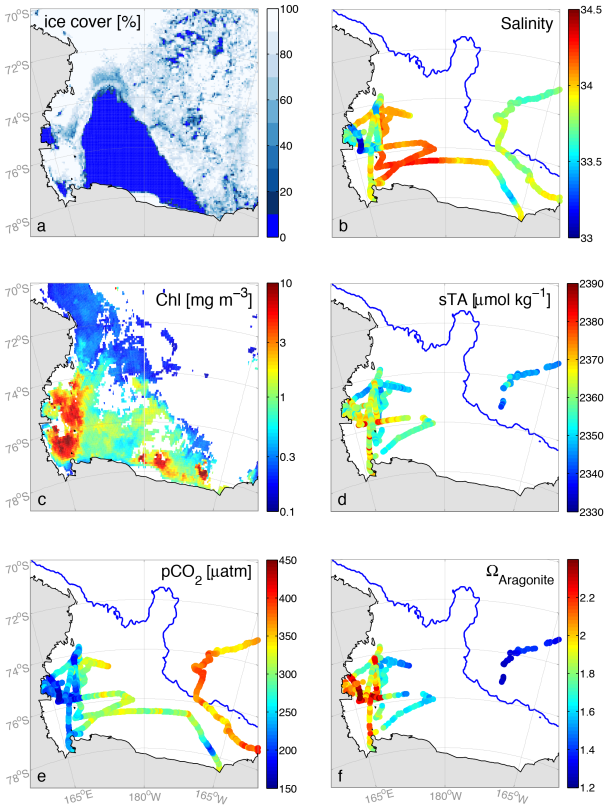

Figure 2. Maps of **(a)** 6.25 km gridded sea ice concentration on 1 December 2012 from the University of Bremen, http://www.iup.uni-bremen.de:8084/amsr2/#Antarctic (Spreen et al., 2008), **(b)** sea surface salinity from NBP 13-02, **(c)** satellite chlorophyll concentration on February 2013 from the 9 km level 3 Aqua MODIS product, http://oceancolor.gsfc.nasa.gov/cgi/l3, **(d)** sTA from NBP 13-02, **(e)** pCO_2 from NBP 13-02 **(f)** aragonite saturation state (Ω_{Ar}) from NBP 13-02.

BGD
12, 8429–8465, 2015

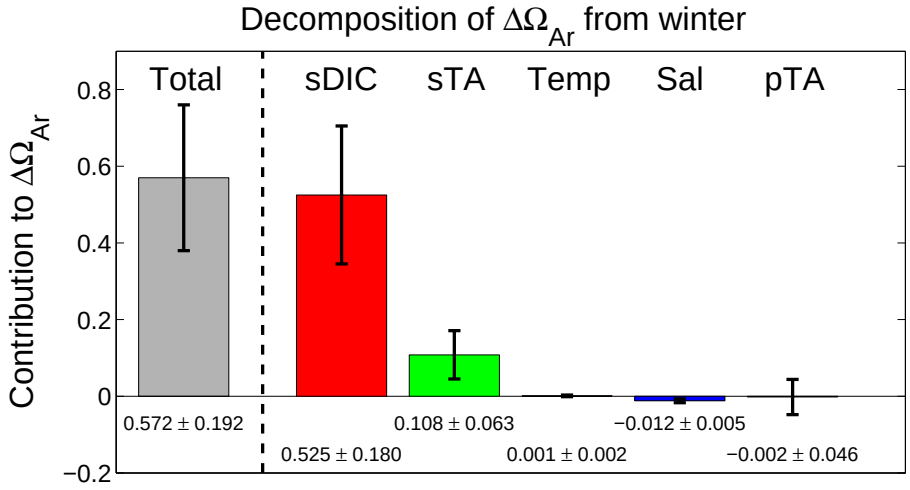

Figure 3. Contributions of sDIC, sTA, temperature, salinity, and pTA to changes in the aragonite saturation state (Ω_{Ar}) of surface waters from the winter to early autumn.

BGD
12, 8429–8465, 2015

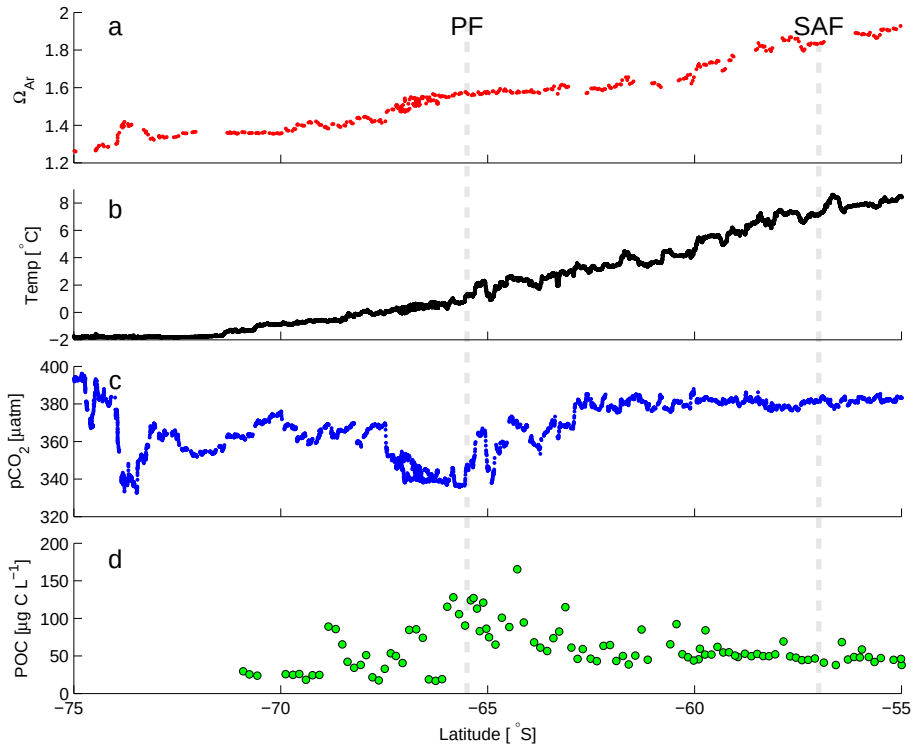

Figure 4. Surface water properties from a Southern Ocean transect, 20 March–2 April 2013: **(a)** aragonite saturation state (Ω_{Ar}), **(b)** SST, **(c)** pCO_2, and **(d)** particulate organic carbon. The Polar Front (PF) and Sub-Antarctic Front (SAF) are indicated (grey dashed lines).

BGD
12, 8429–8465, 2015

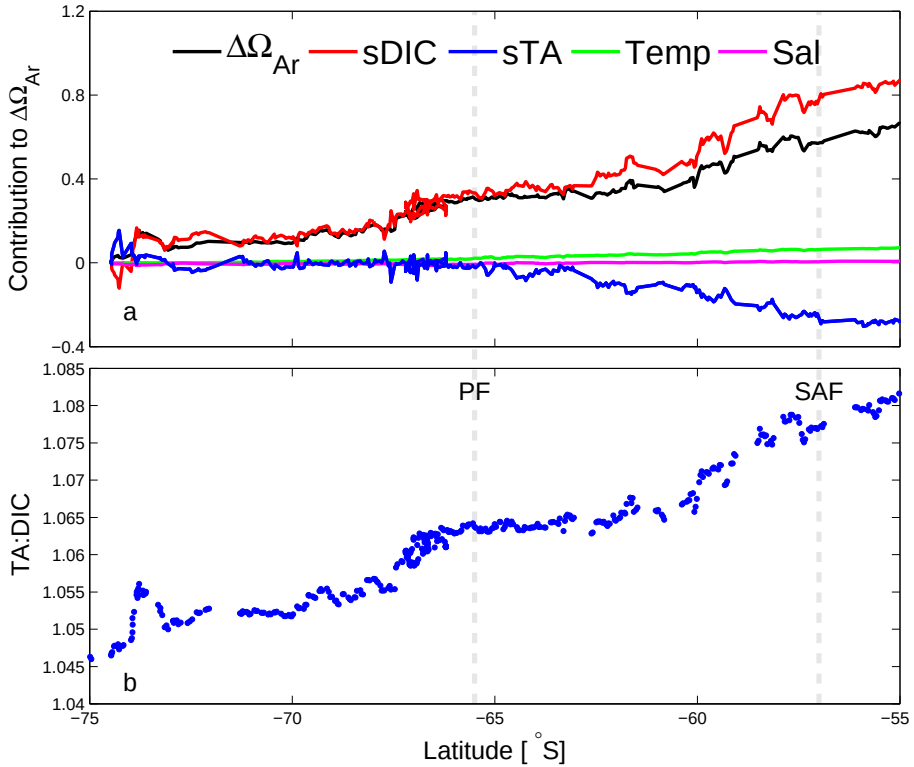

Figure 5. From surface water measurements along a Southern Ocean transect **(a)** contributions of changing sDIC (red), sTA (blue), temperature (green), and salinity (magenta) to changing aragonite saturation state (black, Ω_{Ar}) relative to the start of the transect and **(b)** TA to DIC ratios. The Polar Front (PF) and Sub-Antarctic Front (SAF) are indicated (grey dashed lines).

BGD
12, 8429–8465, 2015

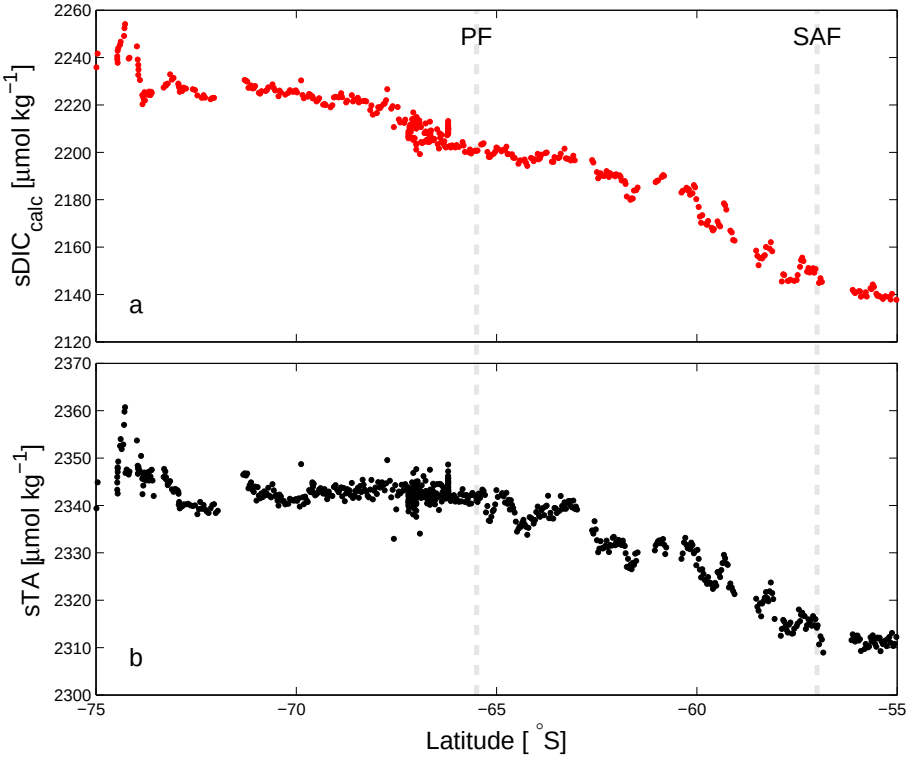

Figure 6. Measured surface water salinity normalized **(a)** DIC calculated from pCO_2, TA, temperature, and salinity and **(b)** TA. The Polar Front (PF) and Sub-Antarctic Front (SAF) are indicated (grey dashed lines).

BGD
12, 8429–8465, 2015

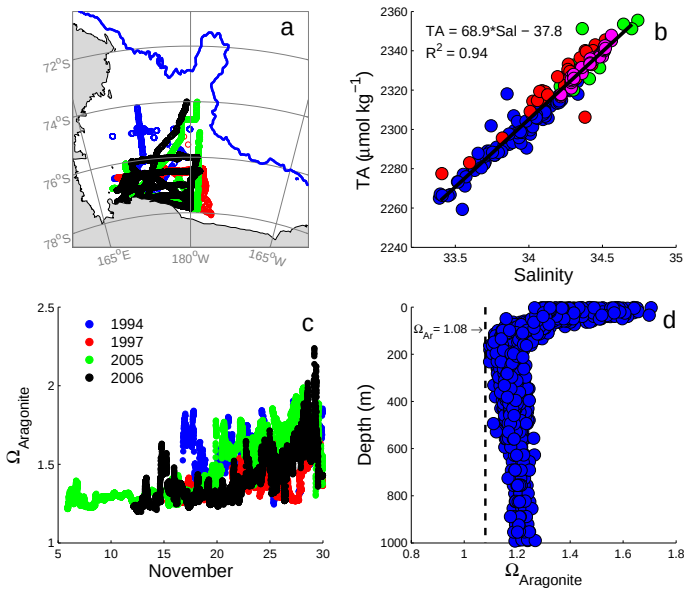

Figure 7. Estimating winter surface aragonite saturation states (Ω_{Ar}): **(a)** map of surface pCO_2 measurements from the LDEO pCO_2 database (http://www.ldeo.columbia.edu/res/pi/CO2) used in this study from November 1994 (blue), 1997 (red), 2005 (green), and 2006 (black). Blue line is the 1000 m isobath. **(b)** Linear regression between TA and salinity with surface data from February–March 2013 (blue, this study), November–December 1994 (green, Bates et al., 1998), December–January 1995/96 (red, Bates et al., 1998), and April 1997 (magenta, Sweeney et al., 2000). TA has been corrected to a nitrate concentration of 29 µmol kg^{-1} to account for the effects of nitrate drawdown on TA (Brewer and Goldman, 1976). **(c)** Aragonite saturation state (Ω_{Ar}) of surface waters from November calculated from pCO_2, salinity derived TA, temperature, and salinity **(d)** profiles of aragonite saturation state (Ω_{Ar}) from off the Ross Shelf (see Fig. 1) from NBP 11-02 calculated from TA, DIC, temperature, and salinity at surface pressures.

BGD
12, 8429–8465, 2015